




A model of quantum gravity on a noisy quantum computer

Muhammad Asaduzzaman ^{1,*} Raghav G. Jha ^{2,†} and Bharath Sambasivam ^{3,‡}

¹*Department of Physics and Astronomy, The University of Iowa, Iowa City, Iowa IA 52242, USA*

²*Thomas Jefferson National Accelerator Facility, Newport News, VA 23606, USA*

³*Department of Physics, Syracuse University, Syracuse, NY 13244, USA*

We study the Sachdev-Ye-Kitaev (SYK) model – an important toy model for quantum gravity on IBM’s superconducting qubit quantum computers. By using a graph-coloring algorithm to minimize the number of commuting clusters of terms in the qubitized Hamiltonian, we find the circuit complexity of the time evolution using the first-order Lie product formula for N Majorana fermions is $\mathcal{O}(N^5 J^2 t^2 / \epsilon)$ where J is the dimensionful coupling parameter, t is the evolution time, and ϵ is the desired precision. This complexity is a significant improvement over existing results in the literature. With this improved resource requirement, we perform the time evolution for $N = 6, 8$ using up to 340 two-qubit gates and perform different error mitigation schemes on the noisy hardware results. We find good agreement with the results obtained using exact diagonalization on classical computers and noiseless simulators. In particular, we compute the return probability to the vacuum state after time t and out-of-time order correlators (OTOC) which is a standard method of quantifying the chaotic nature of quantum many-body systems.

INTRODUCTION

The holographic duality [1] relates a special class of quantum field theories in d dimensions and quantum gravity in $d+1$ dimensions. This strong/weak duality enables one to study the properties of strongly coupled field theory using classical supergravity computations and vice versa. However, there are no cases where both sides of the duality can be studied analytically at the same time. Several attempts have been made on the lattice in Euclidean time using Monte Carlo [2, 3] to study these theories but they have their limitations. Therefore, it is often of interest to find simpler models that have holographic properties and can be studied in the strong coupling limit. One such model which has now been extensively studied is the SYK model [4–7]. It is a model of N interacting Majorana fermions in $0+1$ dimensions with random couplings between q fermions at a time chosen from a Gaussian distribution with zero mean and variance proportional to J^2/N^{q-1} .

An interesting feature of the SYK model is that it develops an approximate conformal symmetry in the large N , low-temperature limit i.e., $N \gg \beta J \gg 1$ (β is the inverse temperature), where it is related to near extremal black holes that develop the $n\text{AdS}_2$ (near AdS_2) geometry. It was shown that this model saturates the chaos bound [8], a feature that is the smoking gun of the holographic (gravity dual) behavior. Since this is a model with all-to-all fermion interactions in $0+1$ dimensions, it is also computationally easier and has been extensively studied up to 60 Majorana fermions [9, 10].

As a potential toy model for understanding quantum gravity, it is, therefore, crucial to study the real-time dy-

namics of this model beyond methods accessible by classical computing methods. This direction has already been explored starting with Ref. [11]. However, they did not perform the computation on real noisy quantum hardware. In another interesting work [12], the authors performed time evolution of a generalized SYK model using a four-qubit NMR quantum simulator and computed bosonic correlation functions and studied the late-time behavior. In addition to the Trotter approach we use in our study, there have been other proposals for time evolution to improve the circuit complexity (beyond the NISQ era) and we refer the reader to Ref. [13] for details.

In this work, we study the SYK model on noisy superconducting quantum computers for the *first* time and put forth an improved circuit complexity¹ to simulate the SYK model on quantum hardware. Specifically, we find an improved complexity from earlier proposals of $\mathcal{O}(N^{10} J^2 t^2 / \epsilon)$ [11] and $\mathcal{O}(N^8 J^2 t^2 / \epsilon)$ [14] to $\mathcal{O}(N^5 J^2 t^2 / \epsilon)$ for the Lie-Trotter-based algorithm [15]. Using this improvement, we study the time evolution of this model up to *eight* Trotter steps on real quantum hardware available through IBM and compute the return probability and four-point out-of-time ordered correlators.

SYK HAMILTONIAN

The Hamiltonian for the SYK model with N -Majorana fermions and q -fermion interaction terms is given by:

$$H = \frac{(i)^{q/2}}{q!} \sum_{i,j,k,\dots,q=1}^N J_{ijk\dots q} \chi_i \chi_j \chi_k \cdots \chi_q, \quad (1)$$

¹ Our definition of circuit complexity is the standard one. The complexity $\mathcal{C}(U)$ is the least number of two-qubit gates in the circuit that implements the unitary time evolution U of a particular Hamiltonian H .

* muhammad-asaduzzaman@uiowa.edu

† raghav.govind.jha@gmail.com

‡ bsambasi@syr.edu

where χ are the Majorana fermions satisfying $\{\chi_i, \chi_j\} = \chi_i \chi_j + \chi_j \chi_i = \delta_{ij}$. We consider the $q = 4$ case with random all-to-all quartic interactions averaged over disorder. The random (real) couplings J_{ijkl} are sampled from a Gaussian distribution with the mean $\overline{J_{ijkl}} = 0$ and variance equal to $\overline{J_{ijkl}^2} = \frac{3!J^2}{N^3}$. We set $J = 1$ in this work. The dimension of the Hilbert space is $\dim(\mathcal{H}) = 2^{N/2}$ where $n = N/2$ is the number of qubits². The SYK model can also be considered for $q > 4$ interactions and is exactly solvable in the large q limit [7].

Qubitization and Trotterization

In order to perform the time evolution of the initial state using the SYK Hamiltonian, we first have to map the fermionic Hamiltonian to qubits. There are different approaches to this encoding in one and higher dimensions. We will use the standard method based on the Jordan-Wigner (JW) transformation. The N fermions, χ (each of size $2^n \times 2^n$) in (1) can be written in terms of tensor product of $N/2$ Pauli matrices X, Y, Z and the identity matrix $\mathbb{1}$ [11, 12] using the JW map as follows:

$$\begin{aligned}\chi_{2k-1} &= \frac{1}{\sqrt{2}} \left(\prod_{j=1}^{k-1} Z_j \right) X_k \mathbb{1}^{\otimes (N-2k)/2}, \\ \chi_{2k} &= \frac{1}{\sqrt{2}} \left(\prod_{j=1}^{k-1} Z_j \right) Y_k \mathbb{1}^{\otimes (N-2k)/2},\end{aligned}\quad (2)$$

where we have suppressed the tensor product between the Pauli matrices to simplify the notation and the factor in front is to ensure the normalization of Majorana as discussed in Ref. [5]. In order to simulate the dynamics on quantum hardware, we first break the Hamiltonian into Pauli strings as $H = \sum_{j=1}^m H_j$ and then use the standard Lie-Trotter formula [16]:

$$e^{-iHt} = \left(\prod_{j=1}^m e^{-iH_j t/r} \right)^r + \mathcal{O} \left(\sum_{j < k} \left\| [H_j, H_k] \right\| \frac{t^2}{r} \right), \quad (3)$$

where we denote the spectral norm by $\|\cdot\|$. If the terms in the decomposition of H are near to commuting, then the Trotter error is greatly reduced and vanishes if they commute. This is usually not the case for interesting physical systems. Though the number of terms into which H is split is $m = \binom{N}{4}$, one can reduce this number by only summing over some small number of clusters of Pauli strings $\mathcal{N} \ll m$. This helps in reducing the Trotter error since the number of terms summed in (3) is reduced. We find that for $N = 6$, the reduction factor i.e., $m/\mathcal{N} = 3$ while for $N = 8$, $m/\mathcal{N} = 35/3$ and this enables us to

² We have $N = 2n$ since two Majorana fermions can be represented by one complex spinless fermion which can be represented by single qubit

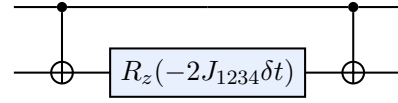


FIG. 1: Circuit implementing one Trotter step of SYK Hamiltonian with $N = 4$ Majorana fermions. The definition of the gate is standard: $R_z(\theta) = \exp(-i\frac{\theta}{2}Z)$.

N	Pauli strings	Clusters	Two-qubit gates
4	1	1	2
6	15	5	30
8	70	6	110
10	210	23	498
12	495	57	1504
14	1001	92	3560
16	1820	116	6812
18	3060	175	11962
20	4845	246	19984

TABLE I: The two-qubit gate cost (assuming all-to-all connectivity) for the time evolution of the SYK Hamiltonian for one Trotter step, number of Pauli strings, and the number of clusters \mathcal{N} of commuting Pauli strings for different N .

reliably evolve to much larger times by controlling the Trotter error considerably (see Supplemental Material for details). If we demand that the total error in simulating the time evolution is ϵ , then we need to perform $r = \mathcal{O}(t^2/\epsilon)$ Trotter steps assuming the spectral norm of commutators to be upper bounded by unity. Using these arguments, Ref. [11] estimated the circuit complexity of $\mathcal{O}(N^{10}t^2/\epsilon)$ but this not optimal. The method based on Lie-Trotter expansion is not the only way of simulating sparse Hamiltonians. A different way is to use the approach where one uses controlled version of oracles to embed the Hamiltonian in an invariant $SU(2)$ subspace method [17] and a variant of this was used in Ref. [13] to bring the cost down to $\mathcal{O}(N^{7/2}t + N^{5/2}t \text{ polylog}(N/\epsilon))$. However, this is not amenable to current hardware implementation. There are also alternatives to Trotter-based simulations in the NISQ-era [18] that are more efficient to implement on quantum hardware [19, 20] but we do not pursue them in this work. We believe it would be interesting to apply these improved techniques to study $N \geq 8$ fermions.

Let us consider the simplest case of $N = 4$. In this case, there is just one Pauli string and we can write the 2-qubit Hamiltonian as $H = -J_{1234}ZZ$ and the time evolution circuit [21] is given by Fig. 1. The two-qubit cost of simulating various N and the number of terms in the decomposition of H can be found in Table I for $N \leq 20$. The circuit complexity estimate based on com-

muting Pauli strings exploiting the graph-coloring algorithm grows³ like $\mathcal{O}(N^5)$, a substantial improvement over $\mathcal{O}(N^{10})$ proposed in Ref. [11]. To obtain this improved scaling, we used well-known methods such as partitioning of the Pauli terms in commuting clusters (using the degree of saturation at each node i.e., DSatur [23] graph-coloring algorithm) and then constructing the diagonalizing operator (circuit) for each cluster [24–28] separately followed by exponentiation for time evolution. At the end we add the gate costs from all clusters [29–31]. The number of Pauli strings in the decomposition of H is given by $\binom{N}{4} = N^4/24 - N^3/4 + 11N^2/24 - N/4$ and grows like $\mathcal{O}(N^4/4!)$ in the large N limit, and the cost to simulate the simplest non-trivial Pauli string of length $N/2$ is $\mathcal{O}(N)$. Hence, it appears that the $\sim N^5$ circuit complexity is close to *optimal* for this approach to Hamiltonian simulation⁴. The complexity can be improved by using Bravyi-Kitaev mapping from fermions, however, such optimizations are not required for small N which are accessible in the NISQ era. We provide details of how we estimate the gate resources in the Supplemental Material (SM) for interested readers.

Return probability

One of the main motivations for using quantum computers is to understand the real-time evolution of complicated quantum many-body systems. An observable we compute in this work is the return probability by evolving an initial state⁵ given by $|\psi_0\rangle = |0\rangle^{\otimes n}$ with the SYK Hamiltonian for N_t Trotter steps and computing the overlap as:

$$\mathcal{P}_0 = |\langle\psi_0|e^{-iHt}|\psi_0\rangle|^2. \quad (4)$$

The return probability is closely related to the spectral form factor [33] and shows similar behavior of slope, dip, ramp, and plateau upon averaging over an ensemble of Hamiltonians [32, 34] which are key features of the SYK model.

The error-mitigated hardware results of the return probabilities for five realizations of the SYK Hamiltonian with $N = 6$ and disorder average are shown in Fig. 2. The dashed black lines are the results from the exact time evolution, while the dashed blue curve is the ensemble average of the exact evolution over the five realizations

of the model. As N increases, the resource requirements quickly increase as shown in Table I. Therefore, for $N = 8$ we consider the time-evolution of just a single instance of the SYK Hamiltonian in Fig. 3. The markers are results obtained from the 127-qubit IBM hardware with various degrees of error-mitigation applied.

We used devices such as `ibm_cusco`, `ibm_nazca` and `ibm_kyoto`. These machines use the `eagle_r3` processor, where the native two-qubit gate is not the standard and familiar CX but the echoed cross-resonance (ECR) gate (see (17) for the definition of the gate). ECR gates are more resilient against error drifting, thereby reducing the need for frequent calibration. The leading source of gate noise in current devices is the two-qubit gates. To deal with this, the error mitigation strategy we employ is a combination of Pauli twirling/randomized compiling [36] for the ECR gates and self-mitigation [37]. For the ECR gate, there is a set of 16 single-qubit conjugations (see SM for details) that leave the exact implementation of the ECR gate invariant, up to a global phase. For each gate implementation, the noise is ‘twirled’ differently for these 16 conjugations. This helps convert a majority of the coherent noise in the circuit into incoherent noise that is well-modeled by the depolarizing quantum channel (see SM for details).

We then construct mitigation circuits with the same structure and gate count as the physics circuits, to characterize the probability of errors p due to the depolarizing channel. With self-mitigation, the idea is to construct a circuit consisting of $N_t/2$ Trotter steps forward in time and $N_t/2$ Trotter steps backward in time. On a noiseless device, this would bring one back to the initial $|\psi_0\rangle$ state, up to Trotter error. However, on a noisy device, the state of the system after the mitigation circuit would be some $|\bar{\psi}_0\rangle$. The probability of error is then $p = |\langle\psi_0|\bar{\psi}_0\rangle|^2$. Using this, we can extract the noiseless return probability $\langle\mathcal{P}_0\rangle$ from the noisy one $\overline{\langle\mathcal{P}_0\rangle}$ using [38]

$$\langle\mathcal{P}_0\rangle = \frac{\overline{\langle\mathcal{P}_0\rangle} - 2^{-n}p}{1 - p}. \quad (5)$$

We build 75 Pauli-twirled physics circuits, and 75 Pauli-twirled self-mitigation circuits and run them each for 2048 shots. We also use the standard M3 protocol [39] for qubit measurement errors and dynamical decoupling [40–43] to suppress decoherence noise. The results for the return probability⁶ with different types of error mitigation applied and exact evolution are shown in panels (a–e) of Fig. 2 for five different instances of the SYK Hamiltonian with $N = 6$ and the disorder average over these realizations is shown in the last panel (f). The return

³ For small N i.e., $N \leq 10$, the two-qubit cost based on quantum Shannon decomposition (QSD) of the unitary matrix $\exp(-iHt)$ is lower [22]. However, it is known to have the exponential scaling for larger N .

⁴ For q SYK Hamiltonian, the complexity will be $\sim \mathcal{O}(N^{q+1})$ (up to factor of $q!$) with first-order product formula and this suggests that beyond some critical q , there won’t be any quantum advantage for simulation of this model

⁵ The initial state chosen here belongs to the set of common eigenstates of the SYK spin operators defined in [32] and forms a complete basis of the SYK Hilbert space

⁶ We only show even Trotter steps because for self-mitigation, one requires forward and backward Trotter evolution by an equal amount

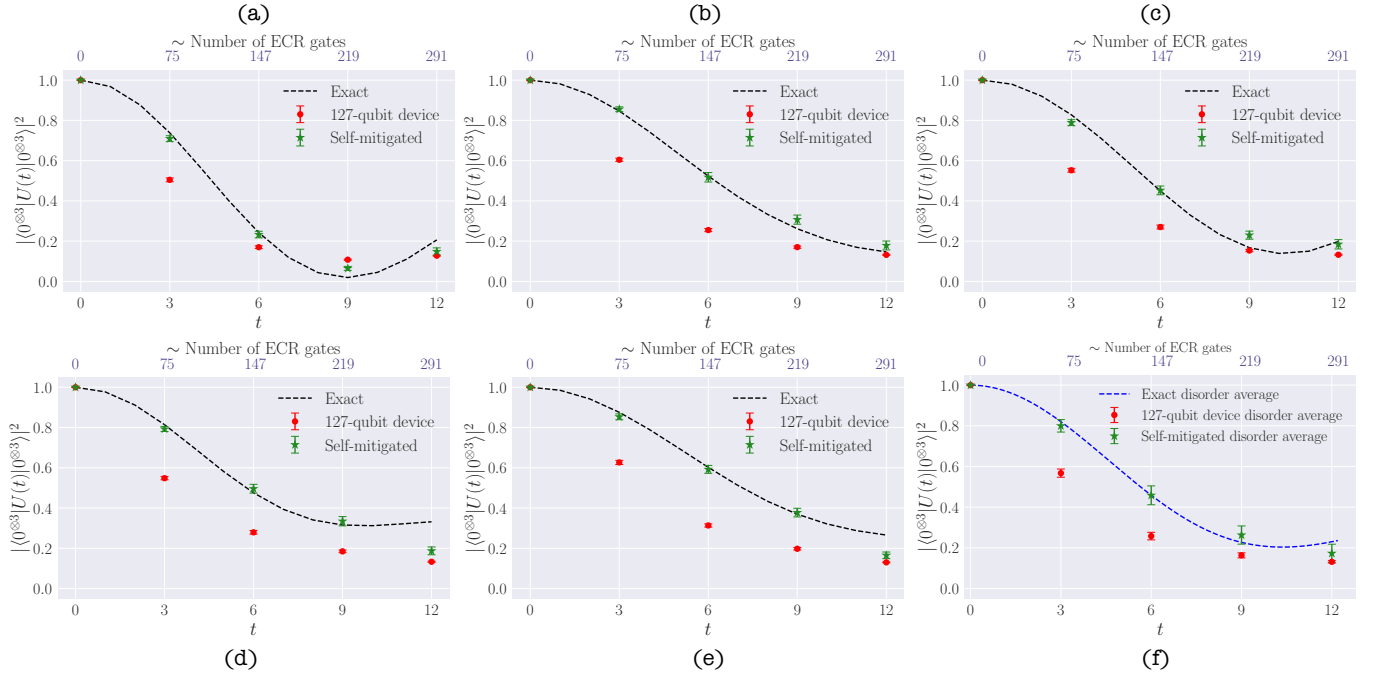


FIG. 2: The return probability computed for five realisations (panels *a* through *e*) of the SYK model with $N = 6$. The error bars are smaller than the symbol size. The disordered average (panel *f*) clearly shows the slope region and the starting of the ramp behavior. The hardware results for the last Trotter step ($t = 12$) were obtained on `ibm_cusco` while all others were obtained on `ibm_nazca`. For each data point on the IBM device, we ran 75 physics circuits and 75 self-mitigation circuits with 2048 shots.

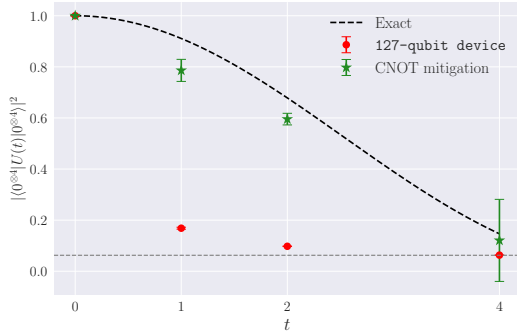


FIG. 3: The return prob computed for a single instance of the SYK model with $N = 8$. The return probability before CNOT only mitigation [35] is slightly above the threshold of the fully depolarized channel (gray dashed line). For $t = 1, 2$ we use $dt = 1$ while for $t = 4$ we use $dt = 2$. For $t = 1$, we use 200 physics and mitigation circuits each with 2048 shots, while for $t = 2, 4$ we use 100 circuits each.

probability for $N = 8$ is shown in Fig. 3 for a single instance on `ibm_kyoto`. The obtained results are consistent with pure noise and therefore we did not study different realizations of the model for this case.

For $N = 6$, the self-mitigated return probability matches the results from exact diagonalization very well even for a relatively large evolution time, and correspondingly large number of ECR gates in the circuit. For this case, we can probe the slope and dip regions robustly and are beginning to see signs of the ramp region. To simulate the SYK model with $N = 6$ up to $t = 12$ (eight Trotter steps), we require about 300 ECR gates. For $N = 8$, we need about 343 ECR gates which is close to the limit of the current state-of-the-art to do two Trotter steps ($t = 2$ with $dt = 1$, $t = 4$ with $dt = 2$) and 170 (for $t = 1$ with $dt = 1$). We show the results in Fig. 3. It appears to be beyond the current capability even with advanced error mitigation methods.

OTOC COMPUTATION

An important feature of the SYK model is that for large N and in the low-temperature limit, it is maximally chaotic and is a quintessential example of a fast scrambler. A defining feature of such systems is that the quantum information shared between a small number of elementary degrees of freedom is rapidly distributed into exponentially many degrees of freedom. This is known as ‘scrambling’. Since black holes are known to be the fastest scramblers in nature, finding similar behavior in a non-gravitational quantum many-body system is highly non-trivial. This is one reason why the SYK model is

considered to be important for understanding aspects of quantum gravity. To quantify this chaos in a quantum system, one considers the out-of-time (OTO) commutator between two operators W and V given by [44–47]:

$$C(t) = -\langle [W(t), V(0)]^\dagger [W(t), V(0)] \rangle, \quad (6)$$

In general $C(t)$ starts from zero, and becomes significant at some later time t , which one refers to as scrambling time (also Ehrenfest time) denoted by t_* . By considering the commutator expansion, we can define the out-of-time order correlators (OTOC)⁷ as:

$$\text{OTOC} := F(t) = \langle W(t)V(0)W(t)V(0) \rangle_\beta, \quad (7)$$

where W and V are generic Hermitian operators and do not have the same symmetry as the Hamiltonian. The growth of the $C(t)$ is related to the decay of the OTOCs i.e., $F(t)$ through the simple relation, $C(t) = 2(1 - F(t))$. The time-evolution of the operator W with Hamiltonian H in the Heisenberg representation is $W(t) = W_t = e^{iHt}W(0)e^{-iHt}$ and $\langle \cdot \rangle_\beta = \text{Tr}\{\rho \cdot\}$ denotes the thermal average with the density matrix ρ at inverse temperature β . A common choice for ρ is to just use the $T \rightarrow \infty$ limit given by the normalized identity matrix, $\mathbb{1}/\dim(\mathcal{H})$ [50] such that $\text{Tr}(\rho) = 1$. For the W and V we can either take Pauli matrices or Majorana fermions such that $W = \chi_i$ and $V = \chi_j$ with $i \neq j$ and average over the different pairs (i, j) . We used the simplest case of a single Pauli matrix, i.e., $W = V = Z$. In what follows, we denote $1 - F(t)$ by $1 - F(t)_{ij} = O_{ij}(t)$ where i and j denote the qubit location of the single-qubit operator W and V respectively and compute this on the hardware. The choice of these operators does not change the basic features of exponential growth and saturation.

The computation of OTOC in quantum many-body systems is useful because it allows for the basis of comparison between black holes and quantum many-body systems without any additional requirements on how the dual gravity theory is fully defined. The OTOC grows as $\exp(\lambda \tilde{t})$ after all two-point correlations (i.e., $\langle W(t)W(0) \rangle$) have decayed (often denoted as t_d) i.e., the exponential growth occurs for $t_d < \tilde{t} \leq t_*$. The exponent λ is known as the Lyapunov exponent. As t increases beyond t_* , the exponential growth of OTOC saturates. The scrambling behavior is often a defining feature of quantum many-body systems with all-to-all (non-local) interactions. In Ref. [8], the authors showed that $\lambda \leq 2\pi/\beta$ for any quantum system. The SYK model exactly saturates this bound at low temperatures. These observables have been extensively studied using classical computing

methods such as exact diagonalization [51, 52]. The current resources do not allow us to access very large values of N or explore finite values of β , but we take a first step at computing these quantities in the simplest setting on the quantum computer in this work. With the available resources, we have been able to simulate six Trotter steps⁸ on quantum hardware.

Results for OTOC

Even though the OTOC seems simple to compute, the experimental/quantum computer measurement of the OTOC is very challenging because of the unusual time ordering. In the first study of its kind, Ref. [53] studied OTOC of local operators for the first time on a nuclear magnetic resonance (NMR) quantum simulator, and soon after it was measured on trapped-ion quantum magnet [54]. In addition to these efforts, to compute OTOC on quantum hardware, we need to define a protocol for performing this measurement. Several proposals have been put forth [55–58] in this regard. We use the protocol proposed by Vermersch *et al.* which computes OTOC only by considering forward time evolution and exploiting the statistical correlations between randomized measurements. This method was recently used to compute modified OTOCs in the Ising spin model on hyperbolic space [59] on IBM hardware. We discuss the details of the global protocol based on randomized measurements in the SM. The protocol measures two independent quantities and from the correlation of the measurements, normalized out of time ordered correlators are computed using the following definition

$$O_{ij}(t) = \frac{\overline{\langle W_i(t) \rangle_{u,k_0} \langle V_j^\dagger W_i(t) V_j \rangle_{u,k_0}}}{\overline{\langle W_i(t) \rangle_{u,k_0}^2}}. \quad (8)$$

The $\overline{\cdot}$ denotes the ensemble average of an operator over a set of unitaries $\{u, v, \dots\}$ and $\langle \dots \rangle_{u,k_0}$ denotes quantum expectation values computed from measurements with a particular unitary u and a chosen initial state $|k_0\rangle$.

The protocol introduces computational overhead due to running circuits for many different unitaries N_u for the computation of each data point. However, some salient features of this protocol make this a suitable choice. The normalized quantity in (8) consists of a ratio, and hence the protocol is robust against depolarizing error and readout errors since this scales the estimated quantities $\langle W(t) \rangle$ and $\langle VW(t)V \rangle$ at the same rate. This resembles the Twirled readout error extinction (T-Rex) error mitigation technique [60] which involves twirling the circuit with Pauli matrices at the end before measurement. The protocol is also robust against imperfect creation of

⁷ These were first introduced in the study of disordered superconductors [48]. OTOC is also closely related to the thermal average of signals from Loschmidt echo as explored in [49]

⁸ All time scales are in units where $J = 1$

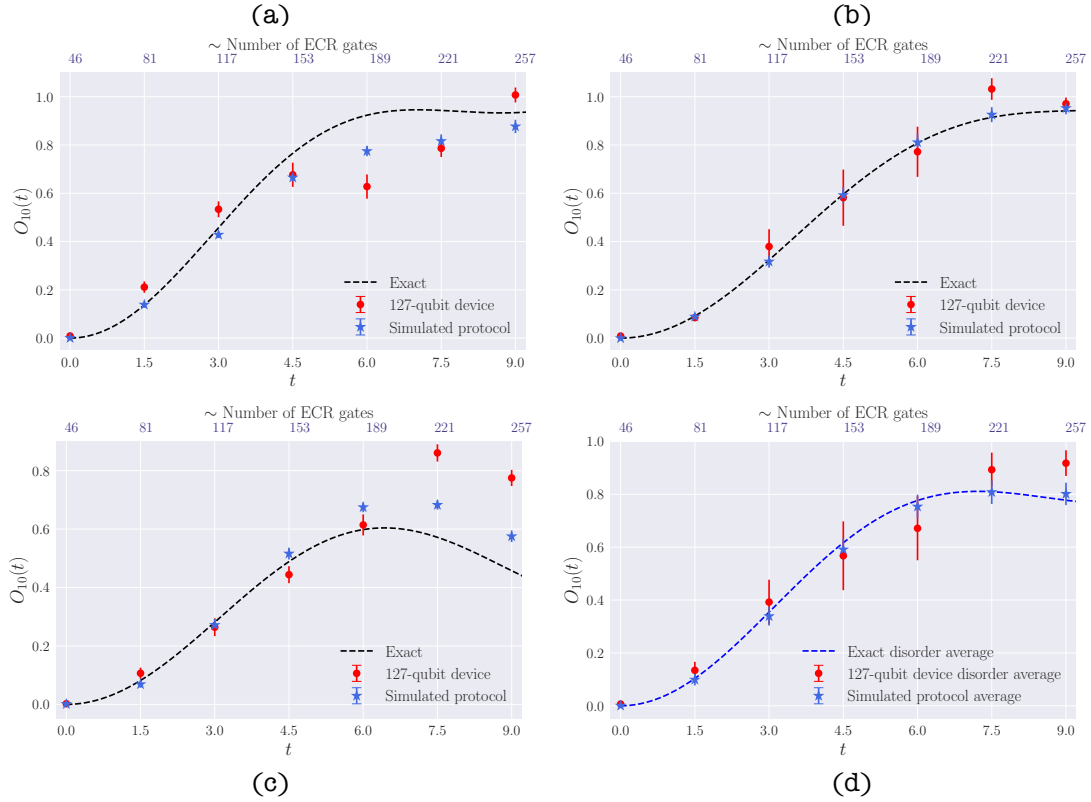


FIG. 4: The OTOC for three realisations (panels *a*–*c*) of the SYK model with $N = 6$ fermions. The disordered average is shown in panel (*d*). Hardware results are obtained on `ibm_kyoto`, and `ibm_cusco` depending on the availability of the device during the run time. We used $N_u = 1100$ unitaries for the measurements of $\langle W \rangle$ and $\langle VW(t)V \rangle$ with $N_M = 4000$ shots per circuit.

the random unitaries [57]. It remains to be seen if the protocol can be made more cost-effective by designing the unitaries with approximate construction like that of unitary t -design [61, 62]. The protocol does not require any ancilla qubits and the backward propagation is not required making it viable for the implementation with the NISQ devices. An extensive study comparing different protocols for the SYK model on hardware is an interesting direction on which we hope to report in the future. The results for OTOC from `ibm_cusco` and `ibm_kyoto` for three instances of $N = 6$ and the disorder average over them is shown in Fig. 4. For this computation, we used the M3 readout error mitigation protocol and dynamical decoupling. Even without the self mitigation, we find good agreement with the exact results. We believe this is due to the robust nature of the protocol against different error channels.

SUMMARY AND DISCUSSION

We have proposed an improved circuit complexity for Hamiltonian simulation of the SYK model with N Majorana fermions from $\mathcal{O}(N^{10}t^2/\epsilon)$ down to $\mathcal{O}(N^5t^2/\epsilon)$ using well-known techniques and performed quantum simulations of the SYK model on noisy quantum comput-

ers. We studied the behavior of return probability due to its close relation to the spectral form factor in the semi-classical limit using 127-qubit `ibm` quantum computers for $N = 6, 8$ Majorana fermions. Due to the noisy devices currently accessible for the computations, we applied state-of-the-art error mitigation methods to the hardware result and showed that it agrees well with the exact time evolution results.

We also computed the out-of-time order correlators which are diagnostic of the chaotic behavior of quantum many-body systems for $N = 6$. Though we cannot study the large N and large β limits and see signs of saturation of the Lyapunov exponent on current NISQ devices, we believe that our work will be useful in future explorations of this model beyond the NISQ era. In this regard, to study quantum chaos on a quantum computer, it might also be useful to study OTOC in simplified models similar to SYK [14, 63–65] that are conjectured to have the same low-temperature, large N dynamics as the pure SYK model we considered here. Another direction for extension of our work is to consider $q > 4$ and explore the resource requirements and time evolution in detail. It would be very useful to study the dynamics of the model over different time scales extending to the plateau region

for the return probability at finite β . These interesting problems would require resources that are beyond the contemporary NISQ-era hardware. We therefore leave these questions for future work. The use of quantum computers for models such as the SYK model in coming decades will not only provide new insights into the holographic principle but also into the interesting world of strange metals and quantum many-body systems [66].

Acknowledgements

MA is supported under the U.S. Department of Energy grant DE-SC0019139. RGJ is supported by the U.S. Department of Energy, Office of Science, National Quantum Information Science Research Centers, Co-design Center for Quantum Advantage (C2QA) under contract number DE-SC0012704 and by the U.S. Department of Energy, Office of Science, Office of Nuclear Physics under contract number DE-AC05-06OR23177. BS is supported in part by the U.S. Department of Energy, Office of Science, Office of High Energy Physics, under Award Number DE-SC0009998. MA and BS would like to thank Jefferson Lab's Quantum Computing Bootcamp for the hospitality where this work started. We thank the IBM quantum hub at Brookhaven National Laboratory for providing access to the IBMQ quantum computers on which the computations were done.

Data Availability Statement

The $N = 6, 8$ SYK Hamiltonian realizations, its decomposition in terms of Pauli strings, and the time evolution circuit as OPEN QASM 2.0 files for single Trotter step can be obtained from Ref. [67].

-
- [1] E. Witten, “Anti-de Sitter space and holography,” *Adv. Theor. Math. Phys.* **2** (1998) 253–291, [arXiv:hep-th/9802150](#).
 - [2] S. Catterall, R. G. Jha, D. Schaich, and T. Wiseman, “Testing holography using lattice super-Yang-Mills theory on a 2-torus,” *Phys. Rev. D* **97** no. 8, (2018) 086020, [arXiv:1709.07025 \[hep-th\]](#).
 - [3] S. Catterall, J. Giedt, R. G. Jha, D. Schaich, and T. Wiseman, “Three-dimensional super-Yang-Mills theory on the lattice and dual black branes,” *Phys. Rev. D* **102** no. 10, (2020) 106009, [arXiv:2010.00026 \[hep-th\]](#).
 - [4] S. Sachdev and J. Ye, “Gapless spin fluid ground state in a random, quantum Heisenberg magnet,” *Phys. Rev. Lett.* **70** (1993) 3339, [arXiv:cond-mat/9212030](#).
 - [5] A. Kitaev, “A simple model of quantum holography,” <http://online.kitp.ucsb.edu/online/entangled15/>.
 - [6] S. Sachdev, “Bekenstein-Hawking Entropy and Strange Metals,” *Phys. Rev. X* **5** no. 4, (2015) 041025, [arXiv:1506.05111 \[hep-th\]](#).
 - [7] J. Maldacena and D. Stanford, “Remarks on the Sachdev-Ye-Kitaev model,” *Phys. Rev. D* **94** no. 10, (2016) 106002, [arXiv:1604.07818 \[hep-th\]](#).
 - [8] J. Maldacena, S. H. Shenker, and D. Stanford, “A bound on chaos,” *JHEP* **08** (2016) 106, [arXiv:1503.01409 \[hep-th\]](#).
 - [9] G. Gur-Ari, R. Mahajan, and A. Vaezi, “Does the SYK model have a spin glass phase?,” *JHEP* **11** (2018) 070, [arXiv:1806.10145 \[hep-th\]](#).
 - [10] B. Kobrin, Z. Yang, G. D. Kahanamoku-Meyer, C. T. Olund, J. E. Moore, D. Stanford, and N. Y. Yao, “Many-Body Chaos in the Sachdev-Ye-Kitaev Model,” *Phys. Rev. Lett.* **126** no. 3, (2021) 030602, [arXiv:2002.05725 \[hep-th\]](#).
 - [11] L. García-Álvarez, I. L. Egusquiza, L. Lamata, A. del Campo, J. Sonner, and E. Solano, “Digital Quantum Simulation of Minimal AdS/CFT,” *Phys. Rev. Lett.* **119** no. 4, (2017) 040501, [arXiv:1607.08560 \[quant-ph\]](#).
 - [12] Z. Luo, Y.-Z. You, J. Li, C.-M. Jian, D. Lu, C. Xu, B. Zeng, and R. Laflamme, “Quantum Simulation of the Non-Fermi-Liquid State of Sachdev-Ye-Kitaev Model,” *npj Quantum Inf.* **5** (2019) 53, [arXiv:1712.06458 \[quant-ph\]](#).
 - [13] R. Babbush, D. W. Berry, and H. Neven, “Quantum Simulation of the Sachdev-Ye-Kitaev Model by Asymmetric Qubitization,” *Phys. Rev. A* **99** no. 4, (2019) 040301, [arXiv:1806.02793 \[quant-ph\]](#).
 - [14] S. Xu, L. Susskind, Y. Su, and B. Swingle, “A Sparse Model of Quantum Holography,” [arXiv:2008.02303 \[cond-mat.str-el\]](#).
 - [15] A. M. Childs, Y. Su, M. C. Tran, N. Wiebe, and S. Zhu, “A Theory of Trotter Error,” *arXiv e-prints* (Dec., 2019) [arXiv:1912.08854](#), [arXiv:1912.08854 \[quant-ph\]](#).
 - [16] S. Lloyd, “Universal quantum simulators,” *Science* **273** no. 5278, (Aug., 1996) 1073–1078, <https://doi.org/10.1126/science.273.5278.1073>.
 - [17] G. H. Low and I. L. Chuang, “Hamiltonian Simulation by Qubitization,” *Quantum* **3** (2019) 163, [arXiv:1610.06546 \[quant-ph\]](#).
 - [18] J. Preskill, “Quantum Computing in the NISQ era and beyond,” *Quantum* **2** (2018) 79, [arXiv:1801.00862 \[quant-ph\]](#).
 - [19] S. Barison, F. Vicentini, and G. Carleo, “An efficient quantum algorithm for the time evolution of parameterized circuits,” *Quantum* **5** (July, 2021) 512, [arXiv:2101.04579 \[quant-ph\]](#).
 - [20] J. W. Z. Lau, T. Haug, L. C. Kwek, and K. Bharti, “NISQ Algorithm for Hamiltonian simulation via truncated Taylor series,” *SciPost Physics* **12** no. 4, (Apr., 2022) 122, [arXiv:2103.05500 \[quant-ph\]](#).
 - [21] A. Kay, “Tutorial on the Quantikz Package,” [arXiv:1809.03842 \[quant-ph\]](#).
 - [22] V. Shende, S. Bullock, and I. Markov, “Synthesis of quantum-logic circuits,” *IEEE Transactions on Computer-Aided Design of Integrated Circuits and Systems* **25** no. 6, (June, 2006) 1000–1010, <https://doi.org/10.1109/tcad.2005.855930>.
 - [23] D. Brélaz, “New methods to color the vertices of a graph,” *Commun. ACM* **22** no. 4, (Apr, 1979) 251–256, <https://doi.org/10.1145/359094.359101>.
 - [24] E. van den Berg and K. Temme, “Circuit optimization of hamiltonian simulation by simultaneous diagonalization of pauli clusters,” *Quantum* **4** (Sep, 2020) 322, <https://doi.org/10.22331/q2f-q-2020-09-12-322>.
 - [25] K. Gui, T. Tomesh, P. Gokhale, Y. Shi, F. T. Chong, M. Martonosi, and M. Suchara, “Term Grouping and Travelling Salesperson for Digital Quantum

- Simulation,” *arXiv e-prints* (Jan., 2020) [arXiv:2001.05983](#), [arXiv:2001.05983](#) [[quant-ph](#)].
- [26] D. Miller, L. E. Fischer, I. O. Sokolov, P. K. Barkoutsos, and I. Tavernelli, “Hardware-Tailored Diagonalization Circuits,” [arXiv:2203.03646](#) [[quant-ph](#)].
- [27] T. Kurita, M. Morita, H. Oshima, and S. Sato, “Pauli string partitioning algorithm with the ising model for simultaneous measurement,” 2022.
- [28] E. M. Murairi and M. J. Cervia, “Reducing Circuit Depth with Qubitwise Diagonalization,” [arXiv:2306.00170](#) [[quant-ph](#)].
- [29] A. Jena, S. Genin, and M. Mosca, “Pauli Partitioning with Respect to Gate Sets,” *arXiv e-prints* (July, 2019) [arXiv:1907.07859](#), [arXiv:1907.07859](#) [[quant-ph](#)].
- [30] V. Verteletskyi, T.-C. Yen, and A. F. Izmaylov, “Measurement optimization in the variational quantum eigensolver using a minimum clique cover,” *J. Chem. Phys.* **152** no. 12, (Mar., 2020) 124114, [arXiv:1907.03358](#) [[quant-ph](#)].
- [31] E. M. Murairi, M. J. Cervia, H. Kumar, P. F. Bedaque, and A. Alexandru, “How many quantum gates do gauge theories require?,” *Phys. Rev. D* **106** no. 9, (2022) 094504, [arXiv:2208.11789](#) [[hep-lat](#)].
- [32] T. Numasawa, “Late time quantum chaos of pure states in random matrices and in the Sachdev-Ye-Kitaev model,” *Phys. Rev. D* **100** no. 12, (2019) 126017, [arXiv:1901.02025](#) [[hep-th](#)].
- [33] Y. Liu, M. A. Nowak, and I. Zahed, “Disorder in the Sachdev-Yee-Kitaev Model,” *Phys. Lett. B* **773** (2017) 647–653, [arXiv:1612.05233](#) [[hep-th](#)].
- [34] J. S. Cotler, G. Gur-Ari, M. Hanada, J. Polchinski, P. Saad, S. H. Shenker, D. Stanford, A. Streicher, and M. Tezuka, “Black Holes and Random Matrices,” *JHEP* **05** (2017) 118, [arXiv:1611.04650](#) [[hep-th](#)]. [Erratum: *JHEP* 09, 002 (2018)].
- [35] M. Urbanek, B. Nachman, V. R. Pascuzzi, A. He, C. W. Bauer, and W. A. de Jong, “Mitigating depolarizing noise on quantum computers with noise-estimation circuits,” *Phys. Rev. L* **127** (2021) 270502, [arXiv:2103.08591](#) [[quant-ph](#)].
- [36] J. J. Wallman and J. Emerson, “Noise tailoring for scalable quantum computation via randomized compiling,” *Phys. Rev. A* **94** no. 5, (Nov., 2016) 052325, [arXiv:1512.01098](#) [[quant-ph](#)].
- [37] S. A. Rahman, R. Lewis, E. Mendicelli, and S. Powell, “Self-mitigating Trotter circuits for SU(2) lattice gauge theory on a quantum computer,” *Phys. Rev. D* **106** no. 7, (2022) 074502, [arXiv:2205.09247](#) [[hep-lat](#)].
- [38] M. Urbanek, B. Nachman, V. R. Pascuzzi, A. He, C. W. Bauer, and W. A. de Jong, “Mitigating depolarizing noise on quantum computers with noise-estimation circuits,” *Phys. Rev. Lett.* **127** (Dec, 2021) 270502. <https://link.aps.org/doi/10.1103/PhysRevLett.127.270502>.
- [39] P. D. Nation, H. Kang, N. Sundaresan, and J. M. Gambetta, “Scalable mitigation of measurement errors on quantum computers,” *PRX Quantum* **2** (Nov, 2021) 040326. <https://link.aps.org/doi/10.1103/PRXQuantum.2.040326>.
- [40] L. Viola and S. Lloyd, “Dynamical suppression of decoherence in two-state quantum systems,” *Phys. Rev. A* **58** (Oct, 1998) 2733–2744. <https://link.aps.org/doi/10.1103/PhysRevA.58.2733>.
- [41] P. Zanardi, “Symmetrizing evolutions,” *Physics Letters A* **258** no. 2, (1999) 77–82. <https://www.sciencedirect.com/science/article/pii/S0375960199003655>.
- [42] D. Vitali and P. Tombesi, “Using parity kicks for decoherence control,” *Phys. Rev. A* **59** (Jun, 1999) 4178–4186. <https://link.aps.org/doi/10.1103/PhysRevA.59.4178>.
- [43] N. Ezzell, B. Pokharel, L. Tewala, G. Quiroz, and D. A. Lidar, “Dynamical decoupling for superconducting qubits: a performance survey,” [arXiv:2207.03670](#) [[quant-ph](#)].
- [44] P. Hosur, X.-L. Qi, D. A. Roberts, and B. Yoshida, “Chaos in quantum channels,” *JHEP* **02** (2016) 004, [arXiv:1511.04021](#) [[hep-th](#)].
- [45] W. Fu and S. Sachdev, “Numerical study of fermion and boson models with infinite-range random interactions,” *Phys. Rev. B* **94** no. 3, (2016) 035135, [arXiv:1603.05246](#) [[cond-mat.str-el](#)].
- [46] A. Kitaev and S. J. Suh, “The soft mode in the Sachdev-Ye-Kitaev model and its gravity dual,” *JHEP* **05** (2018) 183, [arXiv:1711.08467](#) [[hep-th](#)].
- [47] E. Lantagne-Hurtubise, S. Plugge, O. Can, and M. Franz, “Diagnosing quantum chaos in many-body systems using entanglement as a resource,” *Phys. Rev. Res.* **2** no. 1, (2020) 013254, [arXiv:1907.01628](#) [[cond-mat.str-el](#)].
- [48] A. I. Larkin and Y. N. Ovchinnikov, “Quasiclassical Method in the Theory of Superconductivity,” *Soviet Journal of Experimental and Theoretical Physics* **28** (June, 1969) 1200.
- [49] B. Yan, L. Cincio, and W. H. Zurek, “Information scrambling and loschmidt echo,” *Phys. Rev. Lett.* **124** (Apr, 2020) 160603. <https://link.aps.org/doi/10.1103/PhysRevLett.124.160603>.
- [50] C. Sünderhauf, L. Piroli, X.-L. Qi, N. Schuch, and J. I. Cirac, “Quantum chaos in the Brownian SYK model with large finite N : OTOCs and tripartite information,” *JHEP* **11** (2019) 038, [arXiv:1908.00775](#) [[quant-ph](#)].
- [51] Y. Cao, Y.-N. Zhou, T.-T. Shi, and W. Zhang, “Towards quantum simulation of Sachdev-Ye-Kitaev model,” *Sci. Bull.* **65** (2020) 1170–1176, [arXiv:2003.01514](#) [[cond-mat.dis-nn](#)].
- [52] T. Anegawa, N. Iizuka, A. Mukherjee, S. K. Sake, and S. P. Trivedi, “Sparse random matrices and Gaussian ensembles with varying randomness,” [arXiv:2305.07505](#) [[hep-th](#)].
- [53] J. Li, R. Fan, H. Wang, B. Ye, B. Zeng, H. Zhai, X. Peng, and J. Du, “Measuring out-of-time-order correlators on a nuclear magnetic resonance quantum simulator,” *Phys. Rev. X* **7** (Jul, 2017) 031011. <https://link.aps.org/doi/10.1103/PhysRevX.7.031011>.
- [54] M. Gärttner, J. G. Bohnet, A. Safavi-Naini, M. L. Wall, J. J. Bollinger, and A. M. Rey, “Measuring out-of-time-order correlations and multiple quantum spectra in a trapped ion quantum magnet,” *Nature Phys.* **13** (2017) 781, [arXiv:1608.08938](#) [[quant-ph](#)].
- [55] N. Y. Yao, F. Grusdt, B. Swingle, M. D. Lukin, D. M. Stamper-Kurn, J. E. Moore, and E. A. Demler, “Interferometric Approach to Probing Fast Scrambling,” [arXiv:1607.01801](#) [[quant-ph](#)].
- [56] D. Aggarwal, S. Raj, B. K. Behera, and P. K. Panigrahi, “Application of quantum scrambling in Rydberg atom on IBM quantum computer,” [arXiv](#)

- e-prints* (June, 2018) [arXiv:1806.00781](#), [arXiv:1806.00781 \[quant-ph\]](#).
- [57] B. Vermersch, A. Elben, L. M. Sieberer, N. Y. Yao, and P. Zoller, “Probing scrambling using statistical correlations between randomized measurements,” *Phys. Rev. X* **9** no. 2, (2019) 021061, [arXiv:1807.09087 \[quant-ph\]](#).
- [58] X. Mi *et al.*, “Information scrambling in quantum circuits,” *Science* **374** no. 6574, (2021) abg5029, [arXiv:2101.08870 \[quant-ph\]](#).
- [59] M. Asaduzzaman, S. Catterall, Y. Meurice, and G. C. Toga, “Quantum Ising model on two dimensional anti-de Sitter space,” [arXiv:2309.04383 \[quant-ph\]](#).
- [60] E. Van Den Berg, Z. K. Mineev, and K. Temme, “Model-free readout-error mitigation for quantum expectation values,” *Physical Review A* **105** no. 3, (2022) 032620.
- [61] C. Dankert, R. Cleve, J. Emerson, and E. Livine, “Exact and approximate unitary 2-designs and their application to fidelity estimation,” *Physical Review A* **80** no. 1, (2009) 012304.
- [62] Y. Nakata *et al.*, “Quantum Circuits for Exact Unitary t-Designs and Applications to Higher-Order Randomized Benchmarking,” *PRX Quantum* **2** no. 3, (2021) 030339, [arXiv:2102.12617 \[quant-ph\]](#).
- [63] A. M. García-García, Y. Jia, D. Rosa, and J. J. M. Verbaarschot, “Sparse Sachdev-Ye-Kitaev model, quantum chaos and gravity duals,” *Phys. Rev. D* **103** no. 10, (2021) 106002, [arXiv:2007.13837 \[hep-th\]](#).
- [64] M. Tezuka, O. Oktay, E. Rinaldi, M. Hanada, and F. Nori, “Binary-coupling sparse Sachdev-Ye-Kitaev model: An improved model of quantum chaos and holography,” *Phys. Rev. B* **107** no. 8, (2023) L081103, [arXiv:2208.12098 \[quant-ph\]](#).
- [65] M. Hanada, A. Jevicki, X. Liu, E. Rinaldi, and M. Tezuka, “A model of randomly-coupled Pauli spins,” [arXiv:2309.15349 \[hep-th\]](#).
- [66] D. Chowdhury, A. Georges, O. Parcollet, and S. Sachdev, “Sachdev-Ye-Kitaev models and beyond: Window into non-Fermi liquids,” *Rev. Mod. Phys.* **94** no. 3, (2022) 035004, [arXiv:2109.05037 \[cond-mat.str-el\]](#).
- [67] M. Asaduzzaman, R. G. Jha, and B. Sambasivam, “A model of quantum gravity on a noisy quantum computer - notebooks and quantum circuits release,” *Zenodo* (November, 2023) . <https://zenodo.org/record/10202045>.
- [68] J. K. Iverson and J. Preskill, “Coherence in logical quantum channels,” *New Journal of Physics* **22** no. 7, (July, 2020) 073066, [arXiv:1912.04319 \[quant-ph\]](#).
- [69] A. He, B. Nachman, W. A. de Jong, and C. W. Bauer, “Zero-noise extrapolation for quantum-gate error mitigation with identity insertions,” *Phys. Rev. A* **102** no. 1, (2020) 012426, [arXiv:2003.04941 \[quant-ph\]](#).
- [70] P. Nation, “Generating Pauli-twirled circuits in Qiskit,” https://quantum-enablement.org/posts/2023/2023-02-02-pauli_twirling.html.
- [71] X. Chen, T. Zhou, and C. Xu, “Measuring the distance between quantum many-body wave functions,” *Journal of Statistical Mechanics: Theory and Experiment* **2018** no. 7, (2018) 073101.
- [72] M. Asaduzzaman, S. Catterall, G. C. Toga, Y. Meurice, and R. Sakai, “Quantum simulation of the N-flavor Gross-Neveu model,” *Phys. Rev. D* **106** no. 11, (2022) 114515, [arXiv:2208.05906 \[hep-lat\]](#).
- [73] D. C. McKay, I. Hincks, E. J. Pritchett, M. Carroll, L. C. G. Govia, and S. T. Merkel, “Benchmarking Quantum Processor Performance at Scale,” [arXiv:2311.05933 \[quant-ph\]](#).

Supplemental Material (SM) for ‘A model of quantum gravity on a noisy quantum computer’

OPTIMIZING THE TIME EVOLUTION CIRCUIT AND RETURN PROBABILITY

One of the main results of the paper is how to perform efficient time evolution of the model. We now provide details related to optimizing the gate costs of the time evolution based on commuting Pauli strings in the decomposition of the qubit Hamiltonian. Let us take $N = 6$ as an example. In this case, we have a three-qubit Hamiltonian which can be decomposed into 15 Pauli strings each with random coupling taken from a well-defined distribution. The generic Hamiltonian is written as:

$$H = \alpha_1 \mathbb{1}ZZ + \alpha_2 X\mathbb{1}X + \alpha_3 X\mathbb{1}Y + \alpha_4 XXZ + \alpha_5 XYZ + \alpha_6 Y\mathbb{1}X + \alpha_7 Y\mathbb{1}Y + \alpha_8 YXZ + \alpha_9 YYZ + \alpha_{10} Z\mathbb{1}Z \quad (9)$$

$$+ \alpha_{11} ZXX + \alpha_{12} ZXY + \alpha_{13} ZYX + \alpha_{14} ZYY + \alpha_{15} ZZ\mathbb{1},$$

where $\alpha_{1,2,\dots,15}$ are the random couplings for a single realization of the model. By inspection, we find that it is possible to divide the terms of H into five clusters where all Pauli strings in a given cluster commute with each other. The clusters are:

$$\{\mathbb{1}ZZ, ZXX, ZYY\}, \{X\mathbb{1}X, YXZ, ZXY\}, \{X\mathbb{1}Y, Y\mathbb{1}X, Z\mathbb{1}Z\}, \{XXZ, YYZ, ZZ\mathbb{1}\}, \{XYZ, ZYX, Y\mathbb{1}Y\}. \quad (10)$$

Since they commute, they can be simultaneously diagonalized. The diagonalizing unitary circuit for each cluster V , satisfies $V^\dagger H_p V = \tilde{H}_p$ where $p = 1 \dots 5$ and \tilde{H}_p is diagonal and can be written completely in terms of Z and $\mathbb{1}$. Therefore, rather than doing $\exp(-iH_p \delta t)$, one performs $\exp(-i(V \tilde{H}_p V^\dagger) \delta t)$. By making use of the well-known identity:

$$Z \otimes Z = \text{CNOT} \cdot (\mathbb{1} \otimes Z) \cdot \text{CNOT}, \quad (11)$$

we can change two Z 's to a single Z and by repeatedly applying this, we can reduce any Pauli string \tilde{H}_p to single Z . Once we have single Z , then we can use the identity that $e^{itI \otimes \mathbb{P} \otimes I} = I \otimes e^{it\mathbb{P}} \otimes I$, where \mathbb{P} is a single Pauli matrix (X , Y , or Z) because $e^{itI \otimes \mathbb{P} \otimes I} = \cos(t)I \otimes I \otimes I + i \sin(t)I \otimes \mathbb{P} \otimes I = I \otimes (\cos(t)I + i \sin(t)\mathbb{P}) \otimes I = I \otimes e^{i\mathbb{P}t} \otimes I$. Therefore, $\exp(-itI \dots IZ \dots I \dots I) = I \dots IR_z(2t) \dots I \dots I$. As an example, for the first cluster i.e.,

$$H_1 = \alpha_1 IZZ + \alpha_{11} ZXX + \alpha_{14} ZYY, \quad (12)$$

we have the diagonalizing circuit made up of one CX and one Hadamard gate. It is easy to show that:

$$\tilde{H}_1 = \alpha_1 IZI + \alpha_{11} ZIZ - \alpha_{14} ZZZ. \quad (13)$$

For the first term, we do not need any CX gate, just the rotation R_z gate. For the second term, we need two CX for the first and third qubit. For the last term, one would naively expect four CX gates from the basic rule that one needs $2(\nu - 1)$ CX for the Pauli term with Hamming weight ν , but since the terms commute, we can use two CX gates for the second term to bring down the required total cost to 4 CX gates. We need two CX gates for V and V^\dagger adding to a total of 6 CX gates. The circuit for one Trotter step is shown in Fig. 5. The next four clusters require 6,

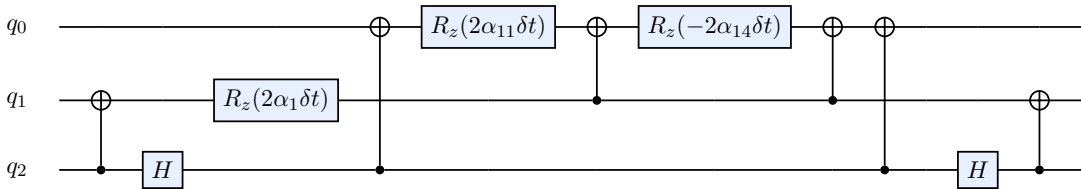


FIG. 5: The circuit to implement $\exp(-iH_1 \delta t)$ for H_1 given in (12) for one Trotter step. The CX and H gates on the left and right end are part of the diagonalizing unitary circuit. The total cost is 6 CX gates as mentioned in the text.

4, 6, and 8 gates respectively, bringing the total cost for $N = 6$ to 30 CX gates as mentioned in Table I for a single Trotter step. If we take the first cluster and do not use the information that can be simultaneously diagonalized, it will increase the circuit complexity. For example, if we just use the optimization levels available in QISKIT, the cost

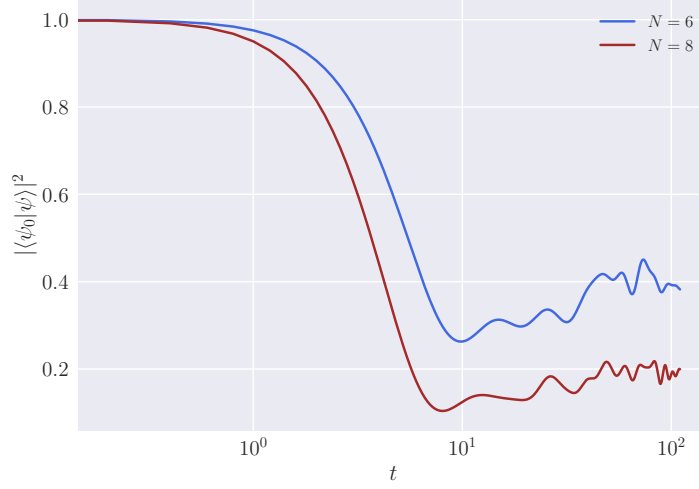


FIG. 6: The exact result for return probability as a function of evolution time t with 100 instances of the SYK model. The initial state is taken to be $|0\rangle^{\otimes n}$. The plateau value $\sim 1/L$ where $L = \dim(\mathcal{H}) = 2^n$ is the dimension of the Hilbert space.

of time evolution for (12) will be 17 CX gates while is about three times more than our estimate. We do a similar procedure for $N = 8$ and find that 70 Pauli terms can be organized into six commuting⁹ clusters each with 14, 12, 8, 14, 12, and 10 terms as given below:

$$\begin{aligned}
& \{11ZZ, ZZ11, 1ZXX, Z1YY, 1ZYY, Z1XX, XX1Z, YYZ1, XXZ1, YY1Z, XYYX, YXXY, XYXY, YXYX\} \\
& \quad \{1XYZ, ZYX1, 1Y1Y, ZXZX, 1ZYX, Z1XY, X1ZY, YZ1X, XZXZ, Y1Y1, XYZ1, YX1Z\} \\
& \quad \{XYYY, YXXX, XYXX, YXYY, XXXY, YYYX, XXYX, YYXY\} \\
& \{1X1X, ZYZY, 1YXZ, ZXY1, 1ZXY, Z1YX, X1X1, XZ1Y, Y1ZX, YZYZ, XY1Z, YXZ1, XXXX, YYYYY\} \\
& \quad \{1X1Y, ZYZX, 1Y1X, ZXZY, 1Z1Z, Z1Z1, X1Y1, XZYZ, Y1X1, YZZX, XXYX, YYXX\} \\
& \quad \{1XXZ, ZYY1, 1YYZ, ZXX1, 1ZZ1, Z11Z, X1ZX, XZ1X, Y1ZY, YZ1Y\}.
\end{aligned} \tag{14}$$

The quantum circuit for the time evolution of $N = 8$ SYK Hamiltonian needs 22, 20, 14, 18, 16, and 20 CX gates per cluster of (14) summing to a total of 110 CX gates per Trotter step. After optimizing the time evolution circuits with δt , we now need to make a good choice of the time step. For this, we did extensive tests of the observables on noise model devices and noiseless simulators and found that $\delta t = 1.5$ is a reasonably good choice. Our results for both return probability and OTOC are in good agreement with this step size. One of the observables we compute on quantum hardware is the return probability (4). Since we focus on the infinite temperature limit ($\beta = 0$) in this work, we do not have access to the standard spectral form factor (SFF). However, for the SYK model, certain features of the SFF are also seen in the return probability as explored in Ref. [32]. We compute the return probability for different N using exact time evolution for $N = 6, 8$. Similar to SFF, one expects to see various stages (referred to as slope and ramp) before it converges to a constant value referred to as a ‘plateau’. The plateau value is the fraction of the initial state retained after sufficiently long time evolution and this depends on the size of the Hilbert space. The slope region is self-averaging (i.e., a single instance of the model shows the same qualitative behavior as the disordered

⁹ Checking whether two Pauli strings of length n commute is straightforward. One needs to check the commutativity of two strings qubit-wise. If the number of qubits denoted by k where they don’t commute is even, the strings commute. Let us consider two six-qubit ($n = 6$) Pauli strings, $XYZZXY$ and

$YX1ZXY$. Only the qubits at the first (X and Y) and second (Y and X) locations don’t commute i.e., $k = 2$. Therefore, the strings commute. It is easy to check that $XYZZXY$ and $YX1ZXX$ don’t commute since $k = 3$.

averaged case) while the ramp and plateau regions for SFF and return probability are not self-averaging. We show the exact results for 100 instances of the evolution in Fig. 6. The slope region for $N = 6$ ends around $t = 10$ and this is consistent with the disorder average over *only* five instances from the hardware results (Fig. 2) in the main text.

ERROR MITIGATION

The usefulness of the noisy intermediate-scale quantum (NISQ) devices is limited by the noise and error that are associated with them. Some common types of errors are — readout errors and gate errors. Readout errors occur when we measure the state of the qubit incorrectly resulting in different probabilities and expectation values. The gate errors are due to the application of gates in a quantum circuit. They are usually classified into coherent and incoherent errors. One useful way of differentiating between coherent and incoherent error is how the infidelity increases with circuit size or the number of times the channel is applied. If it increases linearly, it is a type of incoherent noise. The coherent errors add up quadratically [68]. The coherent errors preserve state purity such that a state that is lying on the surface of the Bloch sphere does not leak in the radial direction and stays pure (on the surface). Incoherent errors map pure states to mixed states such that they can be represented by states inside the Bloch sphere. The incoherent errors are due to the interaction with the outside environment. The incoherent (stochastic) errors are often modeled by the depolarising noise model given by [35]:

$$\mathcal{E}(\rho) = (1 - p)\rho + p\mathbb{1}/2^n, \quad (15)$$

where \mathcal{E} denotes the completely positive trace-preserving map (CPTP) noise channel and ρ is the density matrix and p is the error rate also known as depolarising parameter. If we consider a n -qubit channel, then a probability of $p = 1 - (1/2^n)$ is referred to as ‘completely depolarizing’ or ‘pure noise’ since it destroys the polarization of the qubit and any pure state is changed to a maximally mixed state. The expectation value of an operator \mathcal{O} for the depolarizing channel is given by:

$$\overline{\langle \mathcal{O} \rangle} = \text{Tr}(\mathcal{E}(\rho)\mathcal{O}) = (1 - p)\langle \mathcal{O} \rangle + \frac{p}{2^n}\text{Tr}(\mathcal{O}) \quad (16)$$

The dominant gate errors are coherent (do not spoil unitarity) in nature and hence are not explained by the depolarizing noise channel. However, one can use randomized compiling to transform them into incoherent errors. We do this by inserting a pair of single-qubit gates on both sides such that the two-qubit gate remains unchanged. These possible choices for the ECR gate are shown in Table II. The basis idea of Pauli twirling (also sometimes known as ‘randomized compiling’) [35, 69, 70] is to do operations on two-qubit gates by inserting one-qubit gates from Pauli groups on either side (conjugation) such that the initial gate is left unchanged. The only two-qubit gate we have used is the echoed cross-resonance (ECR) gate which implements:

$$\text{ECR}_{q_0, q_1} = \frac{1}{\sqrt{2}}(IX - XY) = \frac{1}{\sqrt{2}} \begin{pmatrix} 0 & 0 & 1 & -i \\ 0 & 0 & -i & 1 \\ 1 & i & 0 & 0 \\ i & 1 & 0 & 0 \end{pmatrix}. \quad (17)$$

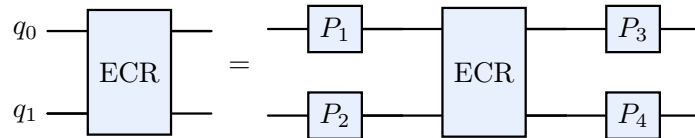


FIG. 7: The circuit implementing the twirling of the ECR gate by choosing the P gates from the Pauli group. This is also sometimes referred to as ‘randomized compiling’. This procedure changes the realistic noise which is coherent in nature to stochastic noise.

As mentioned in the main text, there are 16 conjugations (up to a phase) that leave the ECR gate invariant as shown in Fig. 7. One of them is the trivial conjugation ($P_{1,2,3,4} = \mathbb{1}$). All conjugations ($P_1 \otimes P_2 \cdot \text{ECR} \cdot P_3 \otimes P_4$) are listed below:

P_1	$\mathbb{1}$	X	X	$\mathbb{1}$	Y	Z	Z	Y	Z	Y	$\mathbb{1}$	$\mathbb{1}$	Y	Z	X	X
P_2	$\mathbb{1}$	$\mathbb{1}$	Z	Z	X	X	Y	Y	$\mathbb{1}$	$\mathbb{1}$	X	Y	Z	Z	Y	X
P_3	$\mathbb{1}$	X	X	$\mathbb{1}$	Y	Z	Z	Y	Y	Z	X	X	Z	Y	$\mathbb{1}$	$\mathbb{1}$
P_4	$\mathbb{1}$	$\mathbb{1}$	Z	Z	X	X	Y	Y	Z	Z	Y	X	$\mathbb{1}$	$\mathbb{1}$	X	Y

TABLE II: The 16 conjugations that leave the ECR gate invariant (see Fig. 7). The conjugations in blue yield an overall phase of π .

PROTOCOL FOR OTOC COMPUTATION

For the computation of OTOC as in (7), we have to make a choice of operators, W and V . However, the choice of operators in the four-point function does not change the generic behavior of the growth of OTOC [49]. We studied the exact time evolution using different choices of operators and found that the qualitative difference is not substantial. Due to the limited quantum resources in implementing the OTOC protocol and for benchmarking our results, we have restricted to the simplest choice of W and V i.e., just one non-trivial Pauli matrix in the three-qubit Pauli string.

We follow the Ref. [57] where they discussed a ‘global protocol’ to compute OTOC which uses randomly generated unitaries from the circular unitary ensemble (CUE). By applying random unitaries, many random states are created to mimic a thermalized scenario for the computation of the OTOC. The protocol is developed using the following equation for traceless operators [71],

$$\text{Tr} [W(t)V^\dagger W(t)V] = \frac{1}{N_{\mathcal{H}}(N_{\mathcal{H}} + 1)} \overline{\langle W(t) \rangle_{u,k_0} \langle V^\dagger W(t)V \rangle_{u,k_0}}. \quad (18)$$

On the right-hand side, the overline denotes an ensemble average of measurements over a set $u = \{u_0, u_1, \dots, u_{N_u}\}$ of random unitary operators, k_0 denotes an arbitrary initial state and $N_{\mathcal{H}}$ is the dimension of the Hilbert space. The implementation of the global protocol requires creating a n -qubit random unitary operator that applies to the input state $|k_0\rangle$. The decomposition of an n -qubit random unitary in terms of two-qubit gates scales exponentially with n [22]. For a small number of qubits, the gate cost is manageable with the current NISQ-era machine. We outline the steps to compute OTOC by the randomized protocol developed in Ref. [57] below:

- We prepare an arbitrary initial state $|k_0\rangle$ (position 1 in Fig. 8(a)). For simplicity, we pick the state $|0\rangle = |0\rangle^{\otimes n}$ similar to the calculation of the return probability. Next, we apply a n -qubit random unitary sampled uniformly from the CUE which results in a random state $|\psi_1\rangle = u|0\rangle$ (position 2 in Fig. 8(a)).
- The Trotter evolution of the random state is computed using the Trotterized time-evolution operator $U(N_t) = \left[\exp(-i\hat{H}\delta t) \right]^{N_t}$. This yields $|\psi_2\rangle = U(N_t)|\psi_1\rangle$ at position 3 in the Fig. 8(a).
- Finally, the necessary gates are applied to compute the observable W in the computational basis. For example, if $W = X_i$, an application of the Hadamard gate before applying projective measurements on qubit i in the computational basis would allow us to compute the expectation value of $\langle W(t) \rangle_{k_0, u}$. The number of shots used is denoted as N_M .
- Likewise, the expectation value of the operator $\langle V^\dagger W(t)V \rangle_{k_0, u}$ is computed with an inclusion of the V operator for the same unitary u . The operator is inserted after creating the random state $|\psi_1\rangle$ (position 1 in Fig. 8(b)).
- The process is repeated with N_u unitaries for each Trotter step. We choose N_u either to be 600 or 900 based on convergence. The unitary matrices are drawn randomly from CUE.
- Finally, an ensemble average of the quantity $\overline{\langle W(t) \rangle_{u, k_0} \langle V^\dagger W(t)V \rangle_{u, k_0}}$ is computed which is a measure of the OTOC.

We perform an additional normalization to compute the OTOC with the global protocol

$$O(t) = \frac{1}{\langle W(t) \rangle_{u, \mathbf{k}_0}^2} \overline{\langle W(t) \rangle_{u, \mathbf{k}_0} \langle V W(t) V \rangle_{u, \mathbf{k}_0}}. \quad (19)$$

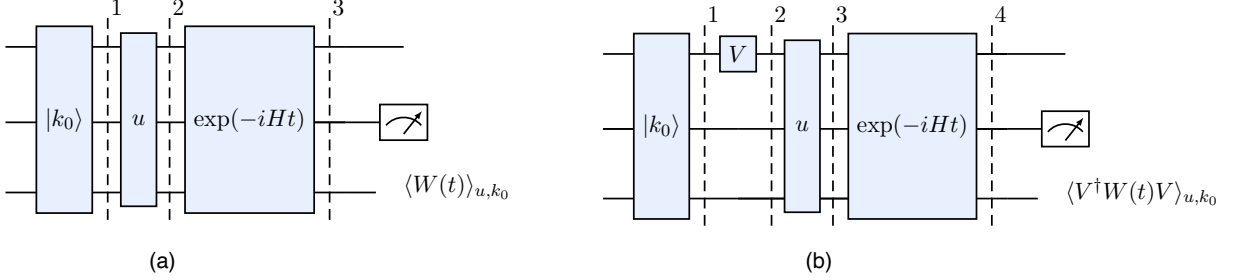


FIG. 8: OTOC is computed from the correlation of the measurement of two different operators (a) $\langle W(t) \rangle$ and (b) $\langle V^\dagger W(t) V \rangle$. The same set of unitaries $\{u_1, \dots, u_{N_u}\}$ are required to find the correlation between the expectation value of the operators.

Following the steps outlined above and using the measurements on circuits like in Fig 8, we can look at the correlation of the computed expectation values. This demonstrates the operator spreading due to information scrambling in the system. The speed of the information spreading can thus be measured with the computation of the OTOC using (19).

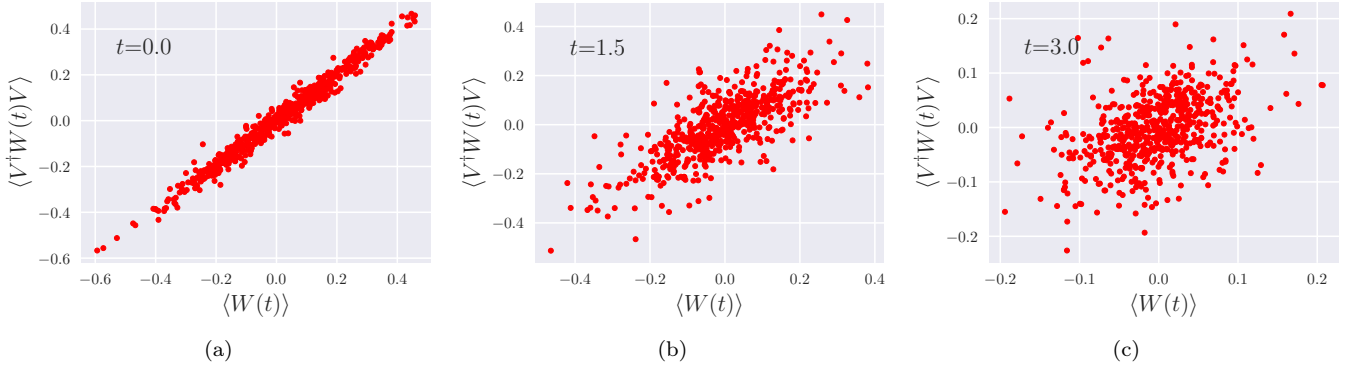


FIG. 9: The change in the correlation of the operators over time in one realization of the $N = 6$ SYK model, with $\langle W(t) \rangle = \langle Z_1(t) \rangle$ and $\langle V W(t) V \rangle = \langle Z_0 Z_1(t) Z_0 \rangle$. Z_i denotes a local Pauli- Z operator on qubit i .

ADDITIONAL DETAILS ABOUT SIMULATIONS ON IBM QUANTUM HARDWARE

Our return probability computation was run on `ibm_nazca`, `ibm_cusco`, and `ibm_kyoto`. The OTOC computation was run on `ibm_cusco` and `ibm_kyoto`. They are all 127 qubit devices with the `Eagle r3` processor. The qubit connectivity of these devices is shown in Fig. 10. All these machines use the same set of basis gates which consist of ECR and single-qubit gates $\{\text{ID}, \text{RZ}, \text{SX}, \text{X}\}$.

We first construct the CNOT circuit for one Trotter step and then append the same circuit $N_t - 1$ times to give the circuit for N_t Trotter steps. We then transpile the circuits to the above basis gate set with the coupling map of the device we used. Though, we only need $(30)N_t$ CNOTs for the entire evolution as discussed in Table I, the actual cost of the two-qubit ECR gate is much higher. This is due to the limited connectivity of the quantum hardware, as shown in Fig. 10. For $N = 6$, we find that about 290 ECR gates are needed for eight Trotter steps, while for $N = 8$, we need about 340 ECR gates for two Trotter steps. Thus it poses a challenge to investigate models with non-local interactions with quantum processing units that have restricted topology. The challenges of restricted qubit topology compared to all-to-all qubit connectivity is discussed in the context of the multi-flavor Gross-Neveu model in [72].

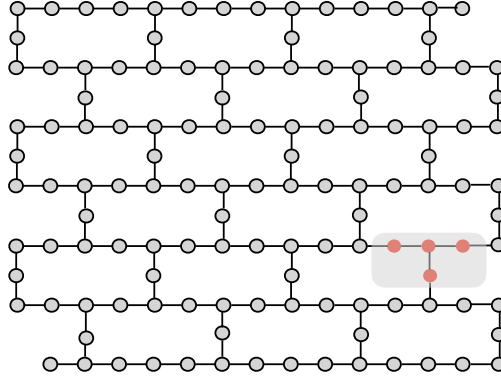


FIG. 10: The general layout of the 127-qubit devices used for this work. We shade a possible option of four utilized qubits (T-configuration) for $N = 8$ which minimizes additional SWAP gates required due to the restricted connectivity of physical qubits.

Other than minimizing SWAP gates required due to restricted topology, we use the following criteria to map physical qubits to virtual qubits

1. Must have low ECR gate error since two-qubit gate errors are the bottleneck in NISQ-era devices.
2. Have a reasonably high coherence time— for a larger number of Trotter steps, we typically need $T_{1,2} \sim 200 \mu\text{s}$.
3. Preferably have a lower ECR gate application time (also sometimes referred to as ‘gate operation time’). This enables us to perform Trotter evolution to larger times.

The typical calibration data of some of the devices used in this work are given in Table III at the time of use (November/December 2023).

Device	EPLG ₁₀₀ [73]	Median T_1 (in μs)	Median T_2 (in μs)	Median ECR gate error
nazca	3.2×10^{-2}	186.8	115.3	1.1×10^{-2}
cusco	5.9×10^{-2}	146.6	83.3	1.74×10^{-2}
kyoto	3.6×10^{-2}	218	115.4	8.52×10^{-3}

TABLE III: Comparison of some important parameters of the 127-qubit devices we have used in this work.

Once good qubits have been chosen, we build the evolution circuits from the Trotter circuits for a given step size. In this work, for the return probability and the OTOC computation, we choose a Trotter step of $dt = 1.5$. We can use sufficiently large Trotter step size primarily because of two reasons:

1. The relevant quantity to consider for Trotter error estimation is $\left(\overline{J_{ijkl}^2}\right)^{1/2} dt \sim \sqrt{3!J^2/N^3} dt$. Due to the small prefactor for $J = 1$, one can choose larger dt .
2. The graph-coloring method reduces the number of terms in the product for Trotterization by grouping the Pauli strings into commuting clusters, thereby reducing the overall error, enabling larger dt .

For the return-probability computation, we also build a self-mitigation circuit, where the system is evolved forward by $N_t/2$ steps, then evolved back by the same number of steps. This circuit would have the same structure as the physics circuit. We then Pauli-twirl each ECR gate in the above circuits and generate 75 versions of the physics and self-mitigation circuits. This makes the coherent errors in the circuit appear stochastic, and well-described by the depolarizing channel upon averaging over all the Twirled circuits. The mitigation circuits can be used to estimate the level of depolarizing noise in the circuit. We run these 150 circuits for 2048 shots each. Then, we compute the noise-less value of the observable as discussed in (5) of the main text.